40th AIAA/ASME/SAE/ASEE Joint Propulsion Conference and Exhibit
11 - 14 July 2004, Fort Lauderdale, Florida

AIAA 2004-4119

Optimization Issues for a Micro-Pulsed Plasma Thruster

Michael Keidar and Iain D. Boyd
Department of Aerospace Engineering, University of Michigan, Ann Arbor MI 48109

In this work we consider several issues related to design of a micro-Pulsed Plasma Thruster (μPPT). One example of such a device has been developed at the Air Force Research Laboratory for delivery of a very small impulse bit. It is concluded that the choice of the optimal energy level for a given micro-PPT geometry is very important. If discharge energy is small, the so called propellant charring would limit the operational time of the thruster. It is found that the charring phenomenon is associated with non-uniformity (in the radial direction between the electrodes) in the propellant ablation rate. On the other hand higher energy leads to discharge constriction on the positive electrode and causes azimuthal non-uniformity. Reasoning leading to such non-uniformity is considered and recommendations for optimal energy and thruster size selections are presented.

I. Introduction

Pulsed plasma thrusters (PPT's) are considered as an attractive propulsion option for stationkeeping and drag makeup purposes for mass and power limited satellites that require μN-s to mN-s impulse bits[1,2]. In particular, the US Air Force has a growing interest in highly maneuverable microsatellites to perform various missions, such as space-based surveillance, on-orbit servicing, inspection, space control etc.[1,2] Recently, an electromagnetic PPT was successfully operated for pitch axis control on the EO-1 spacecraft.[3,4] It was shown that the PPT can be easily scaled down in power and size. A micro-PPT (μPPT) that is the miniature version of the traditional PPT has been designed at the Air Force Research Laboratory (AFRL) for delivery of very small impulse bit.[5,6] The μPPT can deliver a thrust in the 10 μN range to provide attitude control and stationkeeping for microsatellites. In this thruster, the discharge across the propellant surface ablates a portion of the propellant, ionizes it, and then accelerates it predominantly electromagnetically to generate the thrust. It is expected that the use of electromagnetic acceleration to create thrust will also lead to relatively high specific impulse. Even greater miniaturization of the PPT technology was shown recently at Applied Physics Laboratory.[7] They demonstrated microPPT operation at the MEMS scale with an interelectrode gap of only several hundreds μm.

In this paper we consider several issues related to miniaturization of a PPT. It will be shown that the choice of the optimal energy level for a given micro-PPT geometry is very important. If the discharge energy is small, the so-called propellant charring (carbonization) would limit the operational time of the thruster. The charring phenomenon is associated with non-uniformity (in the radial direction between the electrodes) in the propellant ablation rate.[8] On the other hand, when discharge energy is large another discharge non-uniformity occurs or arc-spoking.[9] The plasma typically covers the entire central electrode, but attaches at specific points on the outer electrode resulting in an azimuthal non-uniformity of the discharge as shown schematically in Fig. 1.

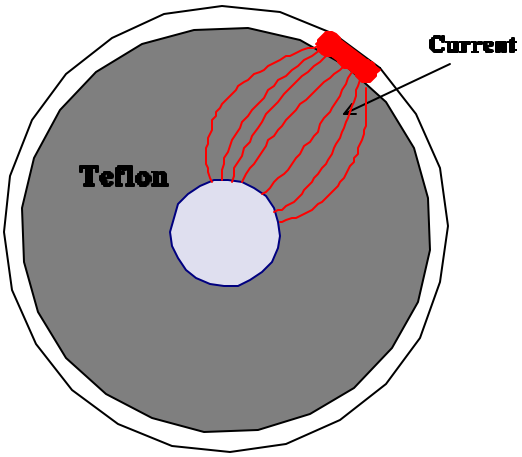

Figure 1: Propellant face showing current non-uniformity in the azimuthal direction

Therefore, the proper choice of the discharge energy and thruster geometry seems to be based on a trade-off between these extreme cases. It is, however, not clear what is the transition point to the extreme regime and what considerations should be involved in the mentioned trade off study. In this paper a model for the trade off study is proposed.

II. Modeling of the current constriction in a micro-PPT

1. Plasma Layer Model

A model of the plasma generation in a micro-PPT was described elsewhere (Refs 8-10, 14). In this paper we briefly outline this model as shown schematically in Fig.2. A fluid model is used since the plasma density near the propellant face is large (in the order of 10^{23}-10^{24} m^{-3}, Refs. 8-10). Mechanisms of energy transfer from the plasma column to the wall of the Teflon™ include heat transfer by particle convection and by radiation. It is assumed that within the plasma layer all parameters vary in the radial direction r. The electron energy balance equation can be written in the form:

$$\frac{3}{2} n \, dT_e/dt = Q_J - Q_r - Q_F - Q_k \qquad (1)$$

where Q_J is the Joule heat and Q_k is the kinetic energy (Q_k=-1/2ΓV^2, Γ is the evaporation rate). A 1D time dependent model of the plasma layer is considered and the equation 1 depends on the coordinate r along the propellant face (see Fig. 2). The radiation heat flux Q_r and particle convection heat flux Q_F depend on the plasma density and temperature[8-10,14]. According to Ref. 11, the radiation in continuum from a C+2F plasma in the considered parameter range provides the main contribution. The radiation energy flux Q_r includes the radiation for a continuum spectrum based on a theoretical model[12,13]. The particle convection flux Q_F includes energy associated with electron and ion fluxes to the Teflon™ and out of the plume that leads to plasma cooling. More details about the model and computational methods can be found elsewhere.[14]

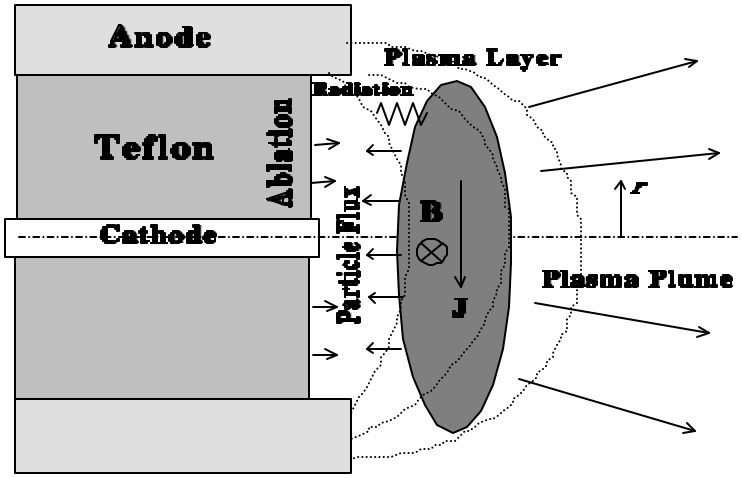

Fig. 2. Schematic of the coaxial micro-PPT electrode configuration

This model is combined with the heat conductivity model. The temperature can be calculated from the heat transfer equation:

$$\frac{\partial T}{\partial t} = a\left(\frac{\partial^2 T}{\partial x^2} + \frac{\partial^2 T}{\partial r^2} + \frac{1}{r^2}\frac{\partial^2 T}{\partial q^2}\right) \qquad (2)$$

where a is the thermal diffusivity, $a=\lambda/C_p\rho$, where λ is the thermal conductivity, C_p is the specific heat capacity and ρ is the specific weight. Eq. 2 is subject to the following boundary conditions[10]:

$$-\lambda\partial T/\partial x(x=0) = q(t) - \Delta H\cdot\Gamma - C_p(T_s-T_o)\,\Gamma \qquad (3)$$
$$\lambda\partial T/\partial x(x=\infty) = 0$$
$$T(t=0)=T_o$$

where x=0 corresponds to the inner dielectric surface, ΔH is the ablation heat, Γ is the ablated flux, T_o is the initial room temperature and q(t) is the density of the heat flux, consisting of the radiative and particle convection fluxes, determined according to Eq. 1 and T_s is the Teflon surface temperature. After the surface reaches some critical temperature, material decomposition begins and ablation heat becomes significant in the energy balance. Heat transfer analysis shows that the temperature profile for the ablated Teflon is exponential[10]:

$$T(x) = T_s\exp(-x\Gamma C_p/\lambda) \qquad (4)$$

Assuming that the thermal conductivity is small, we can reduce Eqs. (2-4) to a 1D problem and therefore we will solve the local heat balance problem.

2. Current Constriction

We will start with an analysis of the arc discharge non-uniformity. Typically, in previous modeling efforts, an azimuthally uniform current sheet has been assumed for simplicity. If the discharge is non-uniform, the current density will increase locally. This in turn will lead to an increase of the heating of the plasma due to Ohmic heat

(which is proportional to j^2, see Eq. 1). As a result, in the local areas of discharge concentration, the heat fluxes to the propellant surface will increase that will in turn lead to locally high surface temperature and ablation rate. On the other hand, the ablated surface area will be smaller and this may also affect the total ablation rate during the pulse.

There are several physical reasons that may lead to discharge non-uniformity, such as current constriction, and cathode and anode spot appearance. The probability of all the mentioned effects increases as the discharge current increases. For instance it was shown[15] that a current increase in the several kA range leads to significant current constriction dependent on the plasma density distribution. The associated effects of the cathode and anode spot generation depend also on the current constriction. Therefore one can expect that an increase in discharge energy (and corresponding current increase) may lead to a high probability of current constriction that will generate azimuthal non-uniformity of the discharge.

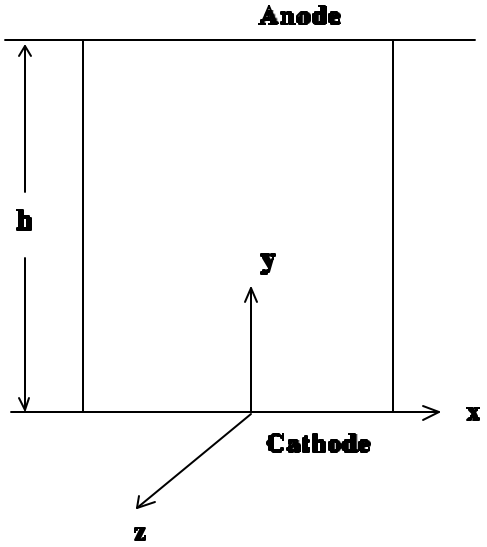

Fig. 3. Schematic of the model geometry

A simple geometry will be adopted for this model as shown in Fig. 3. The current constriction will be modeled in the framework of a hydrodynamic model:

$$\begin{aligned} j &= \frac{1}{m}\nabla B \\ j &= s(-\nabla \boldsymbol{j} - j \times B) \\ \nabla \cdot j &= 0 \end{aligned} \qquad (5)$$

where σ is the plasma conductivity, B is the self magnetic field. It is assumed that the magnetic field has only a z-component and can be calculated from Ampere's law:

$$B_z = -m\int_0^x j_y(x)dx$$

In component form, the system of equations (5) can be written as follows

$$j_x = \sigma\left(-\frac{\partial \varphi}{\partial x} - \frac{j_y B_z}{eN}\right)$$

$$j_y = \sigma\left(-\frac{\partial \varphi}{\partial y} + \frac{j_x B_z}{eN}\right) \qquad (6)$$

where N is the plasma density.

Combining equations (5-6) leads to the following equation for the potential distribution

$$\frac{\partial^2 \varphi}{\partial y^2} + \frac{\partial^2 \varphi}{\partial x^2} - \frac{\beta}{h}\frac{\partial \varphi}{\partial y} - \left(\frac{\partial \varphi}{\partial x} - \beta\frac{\partial \varphi}{\partial y}\right)\frac{2\beta\frac{\beta_o}{h}}{1+\beta^2} = 0 \qquad (7)$$

$$\beta = \frac{\sigma B}{eN}; \qquad \beta_0 = \frac{\sigma}{eN} m j_y h$$

where h is the distance between the electrodes (see Fig. 3), j is the current density, φ is the electric potential, B is the self-magnetic field and N is the plasma density. The problem reduces to solving the equation for the potential distribution in the interelectrode gap with the following boundary conditions: cathode: φ=0; anode: $\varphi = \varphi_a$ (discharge voltage); centerline: $\partial\varphi/\partial x$=0.

The numerical analysis is similar to that developed previously.[15-16] An iterative procedure for finding the plasma density, velocity and potential distribution self-consistently is employed. The equation for potential (Eq. 7) is solved numerically by iteration using the successive overrelaxation procedure. The discharge energy is used as an input parameter for this problem.

The current distribution calculation in the interelectrode gap is shown in Fig. 4. One can see that, due to the effect of the self-magnetic field, the current is constricted near the anode that leads to arc spoking reported earlier.[9] It can be seen that the increase of the discharge energy leads to stronger current constriction.

One can expect that discharge non-uniformity in the azimuthal direction may lead to significant changes of the thruster performance, such as ablation rate. In order to study this effect, a more general model that will include propellant ablation and thermal conductivity of the propellant bulk will be developed. Conditions for the non-uniform discharge operation will be considered below. In addition it is important to note that current constriction affects the current continuity at the anode, i.e. anode spot appearance. This effect is considered in the next section.

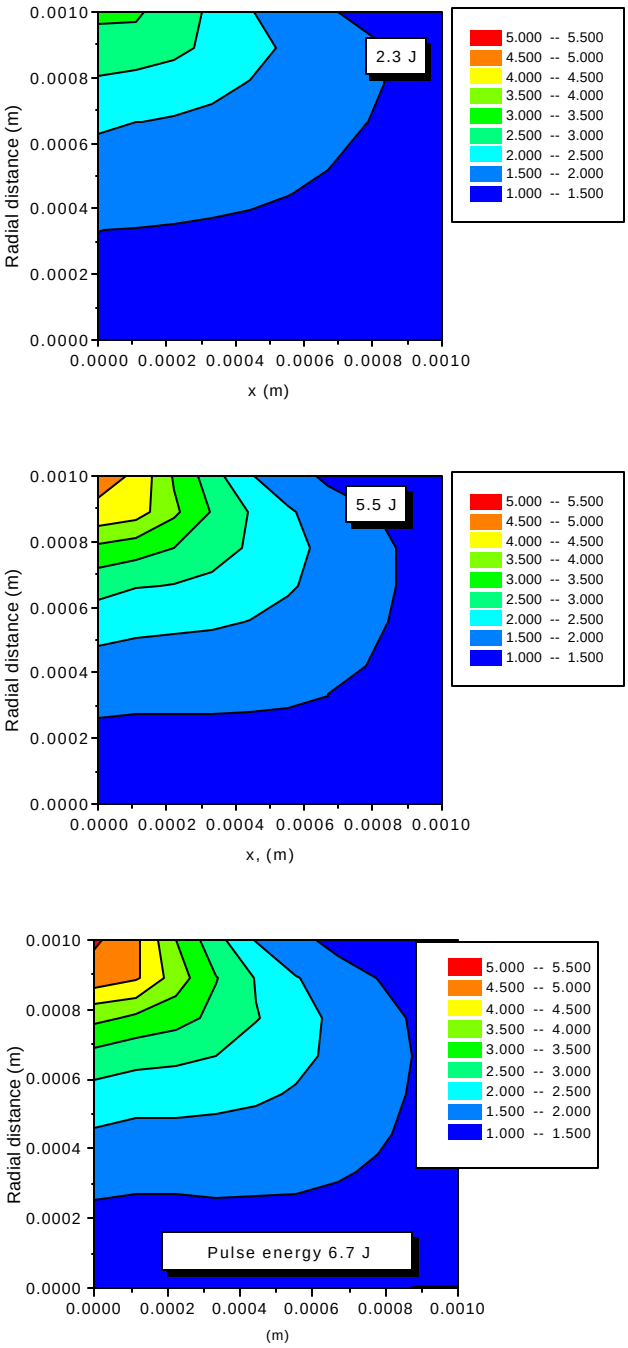

Figure 4: Current density distribution (normalized by the current density at the cathode) showing the current constriction near the upper electrode (anode). Origin of the coordinate system corresponds to the position at the inner electrode radius.

III. Anode spot formation

In this section we describe a model of the near anode region that leads to anode spot formation. Current constriction causes significant increase of the current density near the anode as shown in Fig. 5. Therefore it is important to understand if the current continuity can still be provided. First criterion is related to the electron thermal current near the anode, which is a function of the plasma density.[16] If the thermal current density is smaller than the discharge current density near the anode, the anode current continuity cannot be provided and therefore anode spots may appear.

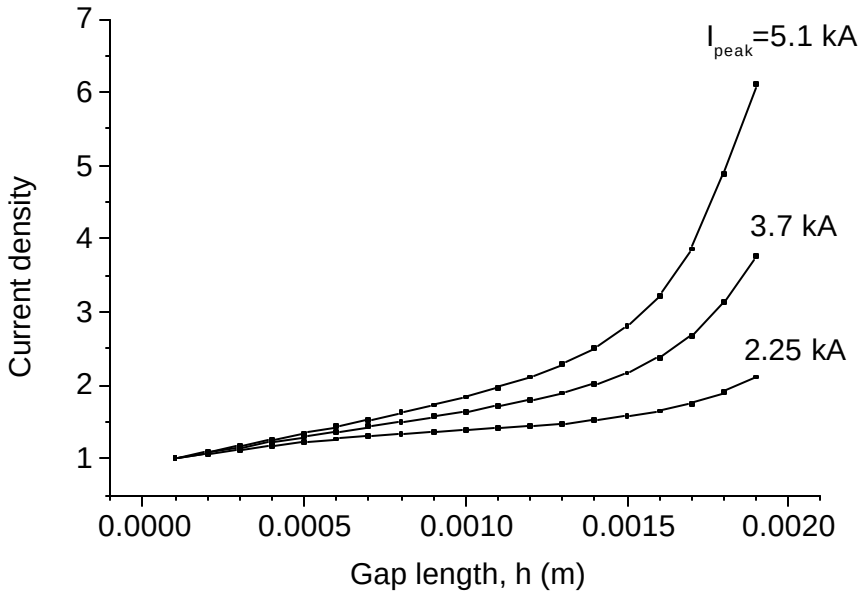

Fig. 5. Current density in the constriction region (normalized by the current density at the cathode).

The calculated plasma density as a function of the current density (according to the plasma layer model described above) is shown in Fig. 6. These calculations are performed for a ¼" diameter micro-PPT operated at 6 J. One can see that the plasma density generally increases with current density and therefore plasma density can provide current continuity even in the constricted region near the anode. However, current constriction leads to an increase of the energy input to the anode and therefore increases in anode heating and local erosion. If the density of the eroded particles (from the anode) approaches the plasma density near the anode, the conditions for anode spot creation can be fulfilled.[17] Let us use the following condition for the anode spot appearance:

$$n_{er}=n_{ea}, \qquad (8)$$

where n_{er} is the density of eroded particles and n_{ea} is the plasma density near the anode, shown in Fig. 6.
The thermal model of the anode used in our calculations is similar to that for the Teflon (see Eqs. 2-4). We are using the following experimental vapor pressure curve for Cu:
$P=10^{A-B/T}$ where A and B are tabulated constants.[18] The heat flux to the anode can be calculated as follows:
$q_a=j_a(2T_e+T_e ln(j_a/j_{eth}))$,

where j_a is the anode current density, j_{eth} is the electron thermal current density and T_e is the electron temperature.

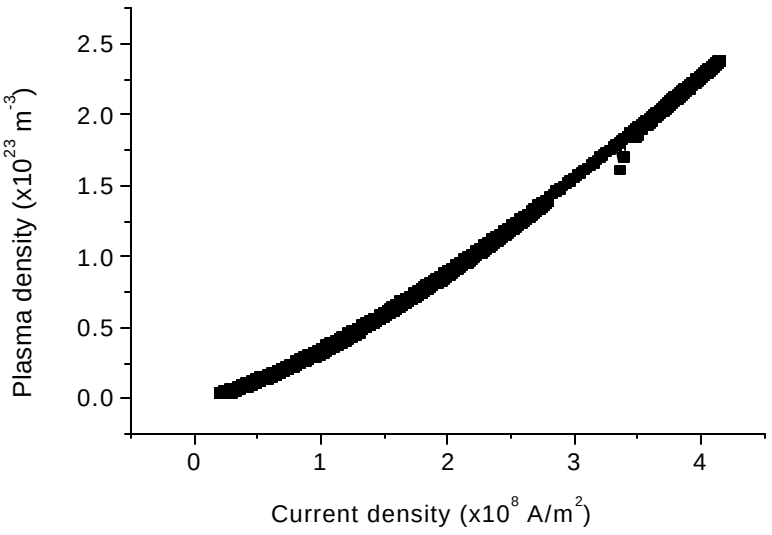

Fig. 6. Plasma density near the anode as a function of the current density

The dependence of the ratio of the eroded density (from the anode) to the plasma density near the anode is shown in Fig. 7 as a function of the combination of the peak current and interelectrode distance with peak current as a parameter. When this ratio reaches 1, one can expect that anode spots will appear (according to Eq. 8). This dependence demonstrates how the criterion for azimuthal uniformity is connected with anode current constriction and anode spot appearance. Conditions for anode spot generation can be created dependent on the peak discharge current and the interelectrode distance. Clearly smaller discharge current and interelectrode distance help to avoid anode spots (and therefore azimuthal non-uniformity). Based on these calculations, the critical peak discharge current for the given thruster geometry or critical thruster size for given peak discharge current can be estimated leading to thruster geometry and discharge optimization, i.e. creation of conditions for azimuthally uniform discharge.

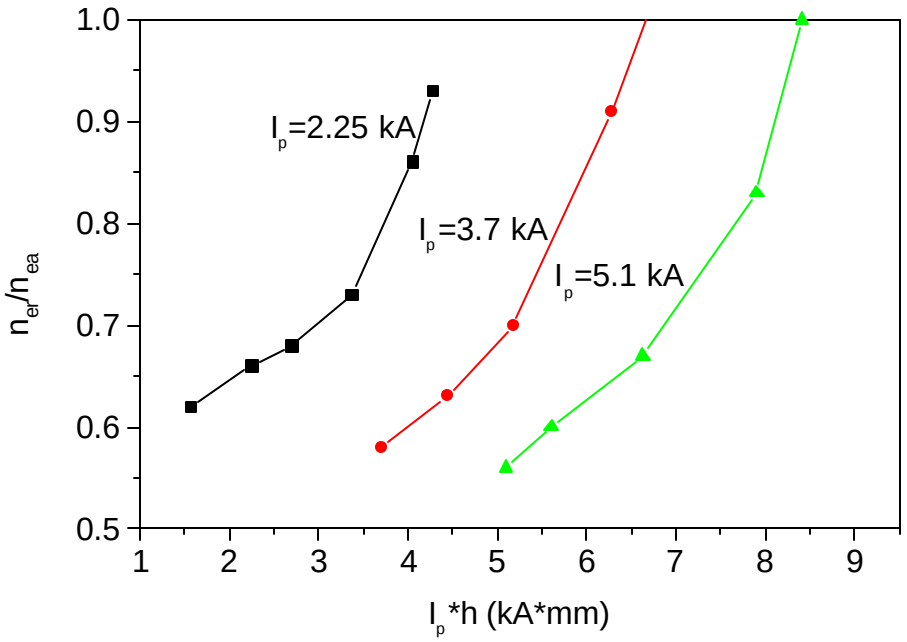

Fig. 7. The anode spot criterion. The dependence of the ration of density of eroded particles to the plasma density near the anode on the peak current and interelectrode distance, *h*.

IV. Ablated mass increase due to non-uniformity

If the discharge is non-uniform, the current density will increase locally. This in turn will lead to an increase of the heating of the plasma due to Ohmic heat (which is proportional to j^2). As a result, in the local areas of the discharge concentration, the heat fluxes to the propellant surface will increase that will in turn lead to locally high surface temperature and ablation rate. On the other hand, the ablated surface area will be smaller and this may also affect the total ablation rate during the pulse. Let us now test this qualitative description using the previously described model (Sec. II). The simplest approach is to use a current density enhancement factor due to discharge non-uniformity as an input condition.

The calculated ablation rate in this case is shown in Fig. 8. As expected, the ablation rate increases with current density enhancement. However some saturation is predicted. This saturation is due to the fact that the propellant surface exposed to the ablation decreases accordingly and while the ablation rate in the area of the discharge concentration is higher, the total ablation rate tends to saturate.

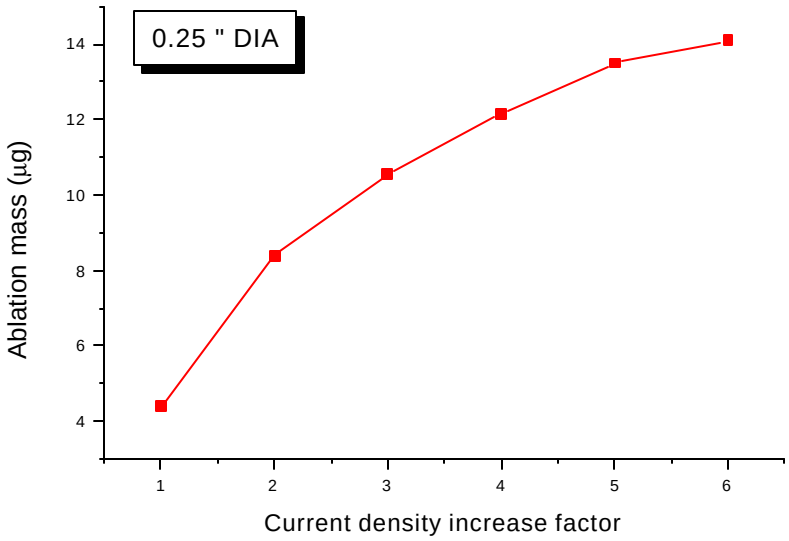

Figure 8. Ablation mass (per single pulse) dependence on current density increase due to discharge non-uniformity in the azimuthal direction.

The possibility of the azimuthal non-uniformity of the discharge in the micro-PPT leads to very high ablation rate as compared with the state-of-the art PPT, such as the LES 8/9. Comparison of the ablation rates for different thrusters is shown in Table 1. For reference, the ablation rate for the electrothermal PPT is also shown.

Table 1. Comparison of the ablated mass LES 8/9 and micro-PPT.

	Ablation rate	Pulse Energy	Specific ablation rate	Reference
LES 8/9	26 μg	20 J	1.3 μg/J	[19]
Micro-PPT (experiment)	6-10 μg	2.5 J	2.4-4 μg/J	5, 6
Micro-PPT (simulation)	4-14 μg	2.5 J	1.6-5.6 μg/J	This work
Elecrothermal PPT (PPT-4)	30-40 μg	10 J	3-4 μg/J	20

It can be seen that the specific ablation rate in the micro-PPT is much higher than that in the state-of-the-art LES 8/9. This effect can be explained in terms of non-uniform ablation as discussed in the previous section.

V. Teflon temperature distribution

In this section we describe the calculation of Teflon surface temperature in the case when the current constriction phenomenon is strong. We calculate the Teflon surface temperature taking into account current density growth in the constricted areas (spots). Teflon surface temperature is calculated (Eqs. 2-4) for two cases inside the spot and outside of the spot. The calculations inside the spot correspond to a discharge peak current of 6 kA that leads to current constriction in the ¼" diameter micro-PPT (see Fig. 4,5).

We will assume that there is current conductivity in the regions outside of the constriction area and the total current fraction outside of the constricted region is used as a parameter (varied between 0.1-0.5 of the total current). After the pulse (about 20 micro-sec) heat propagates inside the propellant and the surface temperature cooling can be described according to the following expression[21,22]:

$$T_s=T_o+(t_p/t)^{0.5}(T_{sp}-T_o) \quad (9)$$

where T_o is the initial temperature, T_{sp} is the Teflon surface temperature at the end of the pulse and t_p is the pulse duration.

Teflon thermal conductivity is not taken into account since it is relatively small and does not affect the results according to our estimations. This allows us to reduce the analysis to the local solution of the heat transfer problem in the constricted region and outside of it.

The calculated results are shown in Fig. 9. It can be seen that in the constricted region the peak of the Teflon surface temperature reaches about 1070 K, while outside of the constricted region it is about 900 K.

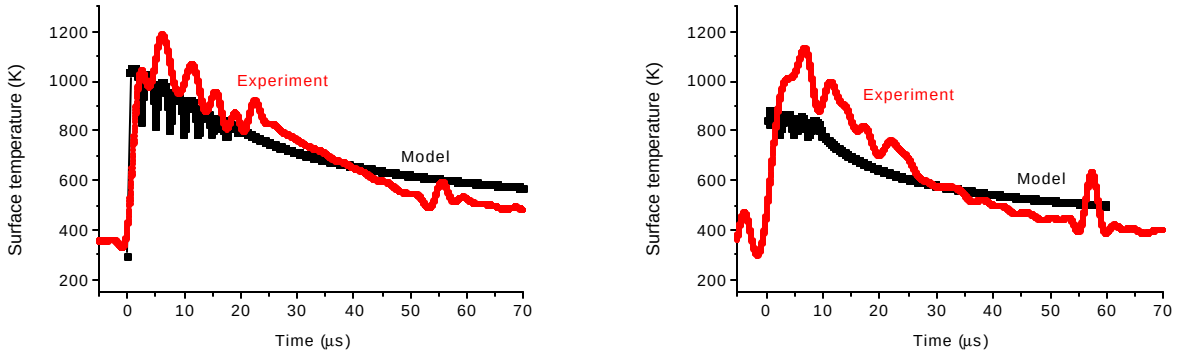

(a) inside the spot (b) outside the spot

Figure 9. Teflon surface temperature inside the spot and outside of the spot. Comparison between simulations and experiment. Experimental results were taken from Ref. 23.

For comparison the experimental results are shown in Fig. 9. The experiment was conducted for a 10 J discharge pulse with peak current of about 6 kA. The surface temperature was measured by phovoltaic infrared detectors.[2224] It should be noted that the experimental results are reliable only after the discharge pulse is gone, which is approximately 20 microsecond. During the discharge the experimental signal is affected by the plasma radiation. One can see that generally good agreement between the experimental results and simulation is obtained for the entire pulse duration for both cases.

VI. Propellant charring dependence on the discharge energy

It was found previously that low energy-to-area ratio leads to Teflon surface charring (Ref. 25, 26). Previous analysis suggests that the charring is associated with carbon atom and ions backflux. Carbon deposition on the Teflon surface leads to film growth. It should be noted that the carbon film is more difficult to evaporate in comparison to the Teflon and therefore when the carbon layer is developed it cannot be evaporated in the typical PPT conditions. Initial discontinuous carbon film growth can be understood by study of discontinuous film growth (see Refs. 27). Carbon film growth (initial island growth) depends on the carbon flux to the surface. An image of the carbon based grown film on the Teflon surface is shown in Fig. 10.

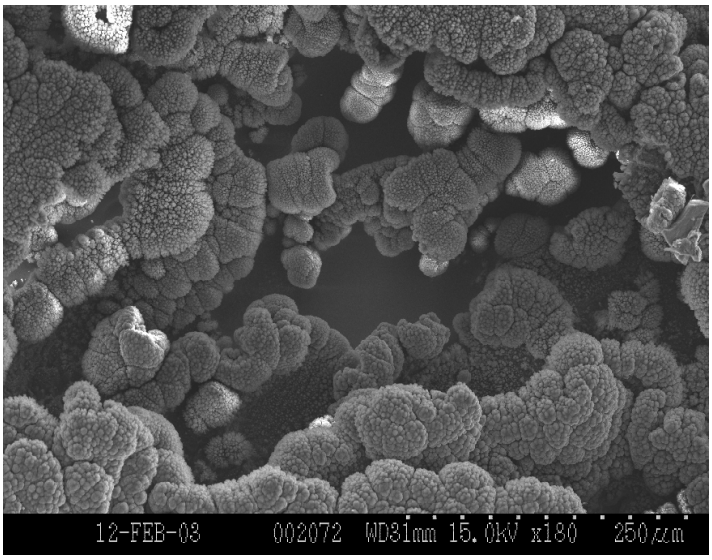

Fig. 10. Scanning electron microscope image of a charred area at the Teflon surface (´180 magnification).

Carbon backflux depends on the conditions at the Knudsen layer edge as was considered in Ref. 28. In this paper we present a calculation for a specific geometry (3.6 mm micro-PPT). The calculated backflux depends on the current density in the vicinity of the Teflon surface. Higher current density leads to plasma acceleration and as a result the velocity at the Knudsen layer edge increases up to the limit of the sound speed.[29] This means that the particle backflux decreases when current density increases. Due to the current spread in the vicinity of the Teflon, the current density is smallest in the region between the electrodes. Therefore one can expect the smallest velocity and as a result the largest backfluxin this area.

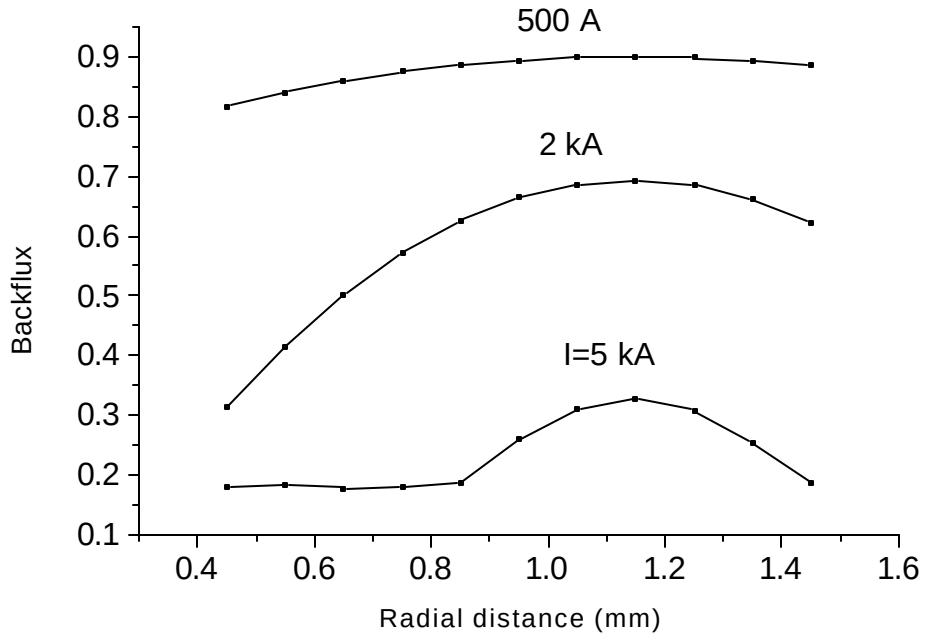

Fig. 11. Dependence of the backflux on the radial position with discharge current as a parameter

These results are shown in Fig. 11. One can see that the highest backflux fraction is predicted to be in the middle of the propellant surface between the electrodes and therefore one can expect that the highest carbon film growth rate will be in this region. This corresponds to experimental finding.[24,25] In addition, it can be seen that in order to achieve a low backflux fraction and therefore a low possibility of carbon char formation, a high discharge current is required.

VII. Effect of the discharge non-uniformity on the thrust bit and specific impulse

In this section we estimate the effect of the discharge non-uniformity on the μPPT performance characteristics such as impulse bit and specific impulse. In the electrodynamic approximation it is assumed that the entire work is done by the circuit to accelerate the moving plasma cloud.[30,31] In this case, the total impulse that can be generated during the pulse can be estimated as follows:

$$\frac{dmU}{dt} = \frac{b}{2} I^2 \qquad (10)$$

where m is the ablated mass, b is the specific inductance in the acceleration channel and I is the instantaneous total discharge current. If the exit velocity is U_e we can estimate the specific impulse from the impulse bit according to relation:

$$I_{bit} = mU_e = mI_{sp}g \qquad (11)$$

It was shown that the total ablated mass increases with current constriction. Thrust bit, I_{bit} , does not depend on the constriction effect since it depends on the total current. Therefore specific impulse will decrease as a result of constriction. So one can conclude that discharge non-uniformity leads to degradation of the thruster performance characteristics and therefore should be avoided.

VIII. Concluding remarks

In this paper we considered some peculiarities related to micro-PPT operation, in particular, dependence on the energy pulse and thruster geometry. It was shown that both discharge energy (peak current) and thruster size affect significantly the discharge uniformity (whether it is azimuthal or radial). Azimuthal non-uniformity relates to the current constriction and anode spot formation phenomena. This happens when the discharge current or thruster size exceed some critical value. Discharge non-uniformity leads to much higher ablation rate and causes degradation of the specific impulse. On the other hand small discharge current leads to strong Teflon surface carbonization (charring), radial non-uniformity, which in turn leads to thruster failure. The primary mechanism of the charring formation was identified and is related to carbon backflux.

Thus the thruster size and discharge energy should be optimized by trading off between two conflicting requirements of the large pulse energy (to prevent charring) and small discharge energy (to prevent current constriction). Since the charring phenomena is completely intolerable, the optimal discharge energy (for a given thruster size) should be chosen somewhere near the spot formation limit. An example of the calculated limit is shown in Fig. 6.

Acknowledgements

The authors gratefully acknowledge financial support by the Air Force Office of Scientific Research through grant F49620-02-1-0084 and by the Air Force Research Laboratory. We also acknowledge D. Bromaghim, E. Antonsen, R.L. Burton, V. Hruby, and L. Byrne for valuable discussions.

References

[1] R. A. Spores, R. B. Cohen and M. Birkan, "The USAF Electric propulsion program", *Proceeding of the 25th International Electric Propulsion Conference*, vol. 1, Worthington, OH, 1997, p.1.

[2] M. Birkan, Formation flying and micro-propulsion workshop, 2002.

[3] J.W. Dunning, S. Benson and S. Oleson, "NASA's electric propulsion program", 27th Inter. Electric Prop. Conf., Pasadena, CA, IEPC-01-002, October 2001

[4] C. Zakrzwsky, S. Benson, P. Sanneman and A. Hoskins"On-orbit testing of the EO-1 Pulsed Plasma Thruster", 38th Joint Propulsion Conference, July 2002, Indianapolis IN, AIAA-2002-3973, July 2002.

[5] Spanjers, G.G., White, D., Schilling, J., Bushman, S., Lake, J., Dulligan, M., "AFRL MicroPPT Development for the TechSat21 Flight," 27th Intl Electric Propulsion Conference, IEPC paper 2001-166, Pasadena, CA 2001.

[6] G. G. Spanjers, D. R. Bromaghim, Capt. J. Lake, M. Dulligan, D. White, J. H. Schilling, S.S. Bushman, E. L. Antonsen, R.L. Burton, M. Keidar and I. D. Boyd, "AFRL microPPT development for small spacecraft propulsion", *38th AIAA Joint Propulsion Conference*, Indianapolis, IN, USA, July 2002, Paper AIAA-2002-3974.

[7] D. H. Simon and H. B. Land, AIAA Paper 2003-5170, July 2003.

[8] M. Keidar, I. D. Boyd, F. S. Gulczinski, E. L. Antonsen, and G. G. Spanjers, "Analyses of Teflon Surface Charring and Near Field Plume of a Micro-Pulsed Plasma Thruster," IEPC Paper 01-155, October 2001.

[9] M. Keidar, I. D. Boyd, E. L. Antonsen, and G. G. Spanjers, AIAA Paper 2003-5166, July, 2003

[10] M. Keidar, I.D. Boyd and I.I. Beilis, "Model of an Elecrothermal Pulsed Plasma Thruster", *Journal Propulsion & Power*, 19, No. 3, 2003, pp. 424-430.

[11] A. I. Zemskov, V. V. Prut, and V. A. Khrabrov, "Pulsed Discharge in Dielectric Chamber", *Sov. Phys. Tech. Phys.*, 17, 1972, pp. 285-289.

[12] G. I. Kozlov, V. A. Kuznetsov, and V. A. Masyukov, "Radiative Losses by Argon Plasma and the Emissive Model of a Continuos Optical Discharge", *Sov. Phys. JETP*, 39, 1974, pp.463-468.

[13] Y. P. Raizer, Gas Discharge Physics, Moscow, Nauka, 1987 (in Russian)

[14] M. Keidar, I. D. Boyd, E. L. Antonsen and G.G. Spanjers, "Electromagnetic Effects in the Near Field Plume Exhaust of a Micro-Pulsed Plasma Thruster", *Journal of Propulsion & Power*, 2004, v. 20, No. 4, July/August.

[15] I. Beilis, M. Keidar, R. L. Boxman, and S. Goldsmith. Theoretical study of plasma jet expansion in a magnetic field in a disc anode vacuum arc. *J. Appl. Phys.*, 83 (2), 1997, pp. 709-717.

[16] M. Keidar, M.B. Schulman and E. Taylor, Model of a diffuse column vacuum arc with cathode jets burning in parallel with a high-current plasma column, IEEE Trans. Plasma Sci., 32, April, 2004, pp. 783-791.

[17] C. Wickert and W. Egli, Theoretical analysis of the current and energy flow to the anode in the diffuse vacuum arc, IEEE Trans. Plasma Sci., 17, pp. 649-652, Oct. 1989.

[18] S. Duschman, Scientific foundations of vacuum technique, New York, Wiley, 1962

[19] R.J. Vondra, K. Thomassen and A. Solbes, Analysis of solid Teflon pulsed plasma thruster, J. Spac. Rockets, v. 7, Dec. 1970, pp. 1402-1406

[20] S.S. Bushman and R.L. Burton, Heating and plasma properties in a coaxial gasdynamic pulsed plasma thruster, J. Prop. Power, V. 17, No. 5, 2001, 959-966

[21] P. J. Turchi, "Directions for improving PPT performance", *Proceeding of the 25th International Electric Propulsion Conference*, vol. 1, Worthington, OH, 1998, pp. 251-258.

[22] M. Keidar, I.D. Boyd and I.I. Beilis, "Electrical discharge in the Teflon cavity of a co-axial pulsed plasma thruster", *IEEE Transaction on Plasma Science*, 28, No.2, 2000, pp. 376-385.

[23] E.L. Antonsen, Ph.D Thesis, University on Illinois Urbana Champaign, May 2004.

[24] E. L. Antonsen, R. L. Burton, G.G. Spanjers, R. A. Spores, Time-resolved surface temperature measurement for pulsed ablative thrusters, IEPC Paper 03-292.

[25] Gulczinski, F., Dulligan, M., Lake, J., and Spanjers, G.G., Micropropulsion Research at AFRL," Paper AIAA-2000-3255, July 2000.

[26] M. Keidar, I.D. Boyd, E. Antonsen, F. Gulchinski, G.G. Spanjers, Propellant charring in Pulsed Plasma Thrusters, J. Prop. Power, v. 20, No. 5, 2004 Sept/Oct.

[27] I. Levchenko, M. Korobov, M. Romanov and M. Keidar, Ion current distribution on a substrate during nano structures formation, *J. Phys. D: Applied Physics*, 37, May, 2004, 1690-1695.

[28] M. Keidar, J. Fan, I.D. Boyd and I.I. Beilis, "Vaporization of heated materials into discharge plasmas", *J. Appl. Phys*., 89, 2001, pp. 3095-3098.

[29] M. Keidar, I. D. Boyd, AIAA Paper 2002-4275, July 2002

[30] A. A. Artsimovich, S. Yu. Luk'ynov, I. P. Podgornyi, and S. A. Chuvatin, Electrodynamic acceleration of the plasmoid. Sov. Phys.-JETP, 6, 33, 1957.

[31] D. Keefer and R. Rhodes, IEPC Paper 97-035, October 1997